Relativistic Electronic Structure in Crystals. II. Fermi Surface of Tungsten*

T. L. Loucks
Institute for Atomic Research and Department of Physics, Iowa State University, Ames, Iowa
(Received 10 September 1965)

The relativistic augmented-plane-wave method developed in the first paper of this series has been applied to tungsten. Relativistic effects on the energy bands and the Fermi surface are presented. The angular dependence of de Haas–van Alphen frequencies, as well as other experimental results, are determined from the theoretical Fermi surface. A comparison with experimental results supports the general conclusion that relativistic effects reduce the size of the Fermi surface of tungsten.

INTRODUCTION

In the first paper of this series[1] (hereafter referred to as THEORY) the derivation was given of a relativistic method for calculating the electronic structure of crystals. This method can be considered a relativistic generalization of the augmented plane wave (APW) method of Slater.[2] For this reason it will be referred to as the RAPW method. The basis function consists of an expansion of 4-component central field orbitals of the Dirac Hamiltonian inside the APW spheres and a Dirac plane wave outside. The choice of the expansion coefficients was discussed in THEORY and the following expression for the matrix elements was developed:

$$M\binom{NM}{n\ m}=(k_N^2-E)\Omega_{nN}\delta_{mM}+4\pi R^2\sum_\kappa D_\kappa\binom{NM}{n\ m}j_l(k_nR)\times\{j_l(k_NR)cf_\kappa(R,E)/g_\kappa(R,E)-j_{l'}(k_NR)k_NS_\kappa\}, \quad (1)$$

where

$$\Omega_{nN}=\Omega\delta_{nN}-4\pi R^2 j_1(|\mathbf{k}_N-\mathbf{k}_n|R)/|\mathbf{k}_N-\mathbf{k}_n|. \quad (2)$$

In this equation $\mathbf{k}_n=\mathbf{k}+\mathbf{K}_n$ where $\mathbf{k}$ is the electron wave vector and $\mathbf{K}_n$ is a reciprocal lattice vector. E is the characteristic energy in the secular equation. The unit cell volume is Ω, and R is the radius of the APW spheres. The κ summation is over positive and negative integers (not zero). The following rules specify l and l':

$$\begin{aligned} l&=\kappa \quad \text{and} \quad l'=\kappa-1, \quad (\kappa>0),\\ l&=-\kappa-1 \quad \text{and} \quad l'=-\kappa, \quad (\kappa<0). \end{aligned} \quad (3)$$

Spherical Bessel functions of order l are written $j_l(x)$. S_κ is the sign of κ. The geometric coefficients are given by

$$D_\kappa\binom{N+}{n+}=|\kappa|P_l(\hat{N}\cdot\hat{n})-iS_\kappa(\hat{N}\times\hat{n})_z P_l'(\hat{N}\cdot\hat{n}), \quad (4)$$

$$D_\kappa\binom{N-}{n+}=-S_\kappa P_{l'}'(\hat{N}\cdot\hat{n})\{(\hat{N}\times\hat{n})_y+i(\hat{N}\times\hat{n})_x\}, \quad (5)$$

where $P_l(x)$ is the Legendre polynomial of order l, and the prime indicates differentiation with respect to the argument x. Equation (4) is for parallel spins and Eq. (5) for antiparallel spins. The orbitals $c_{f\kappa}$ and g_κ in Eq. (1) are regular solutions (at the origin) of the following coupled first-order differential equations[3]:

$$\frac{d(cf)}{dr}=\frac{(\kappa-1)}{r}cf-(E-V)g, \quad (6)$$

$$\frac{dg}{dr}=\left(\frac{E-V}{c^2}+1\right)cf-\frac{(\kappa+1)}{r}g. \quad (7)$$

The potential enters the matrix element only as the ratio of these orbitals evaluated at the APW sphere radius.

In the most recent application of the RAPW method the energy bands in lead were determined.[4] These results were found to be in close agreement with the energy bands based on a model given by Anderson and Gold.[5] This model, which included spin-orbit effects, was based on the comparison of their extensive de Haas–van Alphen data with the results from a four-parameter model based on the pseudopotential formalism. The parameters were adjusted to give the best (in a least-squares sense) agreement between the model and the experimental results. The energy bands calculated from first principles using the RAPW method were in very good agreement with those predicted by this model, especially near the Fermi energy.

The RAPW method was originally developed to study the splitting of energy bands in tungsten.[6] In this application only the symmetry axis ΓH was considered. These results are shown in Fig. 1. The splitting indicated on this figure by the separation bc was found to be in close agreement with the results obtained from the size-effect measurements of Walsh and Grimes.[7]

The calculations for tungsten have now been extended throughout the Brillouin zone in order to determine the relativistic Fermi surface. Extremal cross-sectional

* Work was performed at the Ames Laboratory of the U. S. Atomic Energy Commission. Contribution No. 1783.
[1] T. L. Loucks, Phys. Rev. **139**, A1333 (1965).
[2] J. C. Slater, Phys. Rev. **51**, 846 (1937).
[3] In atomic units with $e^2=2$, $m=\frac{1}{2}$, and $h=2\pi$, the speed of light c is 274.
[4] T. L. Loucks, Phys. Rev. Letters **14**, 1072 (1965).
[5] A. R. Anderson and A. V. Gold, Phys. Rev. **139**, A1459 (1965).
[6] T. L. Loucks, Phys. Rev. Letters **14**, 693 (1965).
[7] W. M. Walsh and C. C. Grimes, Phys. Rev. Letters **13**, 523 (1964).

areas of the Fermi surface have been measured, and the theoretically predicted de Haas–van Alphen frequencies are presented for magnetic field directions in the (011) plane. These and other results are compared with various experimental results, and it is concluded that relativistic effects reduce the size of the Fermi surface.

RESULTS

A complete discussion of the procedure used in constructing the muffin-tin potential has been given in a paper[8] on the nonrelativistic Fermi surfaces of Cr, Mo, and W (hereafter referred to as NON-REL). The same APW sphere radius and lattice constant given in NON-REL were used for the present calculations. The potential for the relativistic calculation was constructed using the relativistic atomic calculations of Liberman, Waber, and Cromer.[9] The procedure for performing RAPW calculations was outlined in THEORY. For this particular calculation a basis set of 39 RAPW's was used. For each of these a spin-up and spin-down component was included yielding a matrix of order 78. The κ summation for each of these matrix elements was truncated at $\kappa=\pm 10$.

1. Fermi Surface of Tungsten

The Brillouin zone for the body-centered cubic lattice is shown in Fig. 2. Cross sections of the Fermi surface of tungsten as given in NON-REL are reproduced in Fig. 3. The nonrelativistic surface consists of four different pieces. There is a large electron surface centered at Γ which resembles a child's jack. A hole surface centered at H has the shape of an octahedron with slightly rounded edges. It has about the same volume as the electron jack. Smaller pieces consist of six equivalent electron "lenses" inside the "necks" of the electron jack. The neck is the restriction between the knobs and the octahedral body of the jack. In addition there are six equivalent hole ellipsoids located at N.

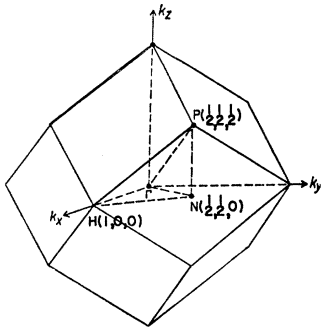

FIG. 2. Brillouin zone for the body-centered cubic lattice.

Cross sections of the relativistic Fermi surface are shown in Fig. 4. Both the electron "lenses" and the holes at N have disappeared. The electron jack and the hole octahedron no longer touch along the ΓH axis. They are separated by the distance bc shown in Fig. 1. The jack has been reduced in size and the necks have been smoothed out by the spin-orbit interaction.

2. de Haas–van Alphen Frequencies

A scale model of the electron jack was made using the cross sections of Fig. 4 and one additional slice located halfway between the planes ΓPH and ΓNH. A photograph of the model is shown in Fig. 5. Because of the extensive computing required to evaluate these cross sections, it was decided to use this scale model to determine extremal areas rather than to compute them numerically. To accomplish this another model like the one in Fig. 5 was constructed out of brass, and the regions between the ribs were filled with plaster. This was then sanded and filed until the edges of the brass fins were exposed and the surface was smooth. This model was mounted with a particular orientation and the cross-sectional areas of horizontal slices through the surface were measured. A typical set of results is shown in Fig. 6 for the magnetic field oriented 65° from the (001) direction in the (011) plane. The extremal areas

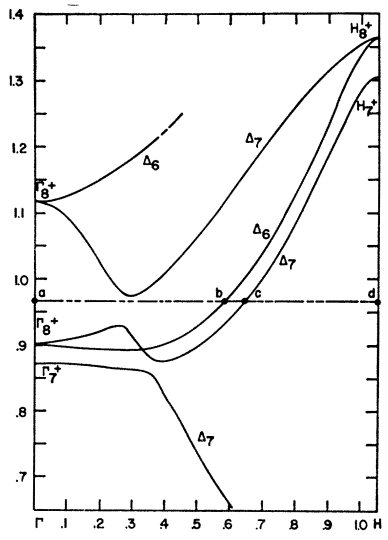

FIG. 1. Relativistic energy bands for tungsten (Ref. 6).

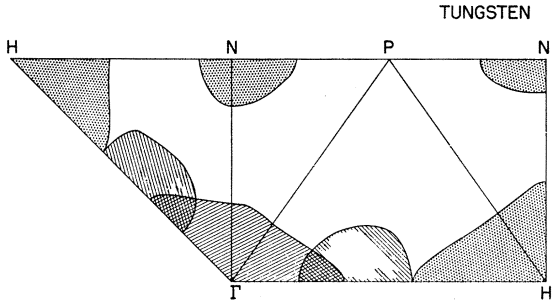

FIG. 3. Nonrelativistic Fermi surface of tungsten (Ref. 8).

[8] T. L. Loucks, Phys. Rev. **139**, A1181 (1965).
[9] D. Liberman, J. T. Waber, and Don T. Cromer, Phys. Rev. **137**, A27 (1965).

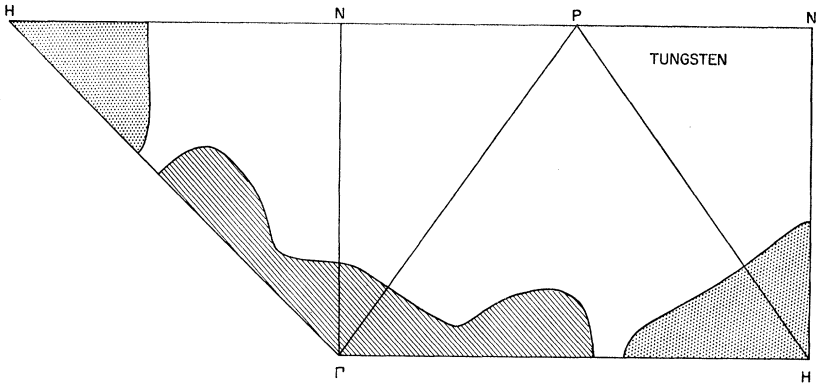

FIG. 4. Relativistic Fermi surface of tungsten.

were converted to de Haas–van Alphen frequencies using the Onsager relation. The results for magnetic field orientations in the (011) plane are given in Fig. 7.

This method of determining the extremal cross-sectional areas is probably not accurate to more than $\pm 5\%$. It was decided, however, that the advantages of direct experience with an almost-to-scale model were more important than having precise theoretical values. It is clear from the complexity of Fig. 6 that it would not be easy to predict extremal areas simply by a casual glance at the cross sections given in Fig. 4.

3. Assorted Other Results

The Fermi energy E_F was determined by the requirement of equal hole and electron volumes. The value is given in Table I along with the result from NON-REL. It was only necessary to determine the constant-energy surfaces for two values of the energy before the hole and electron volumes were found to be nearly equal (Fig. 8). The slopes of these volume curves can be used to calculate the density of electronic states at the Fermi energy $G(E_F)$ (factor of 2 included for spin degeneracy). This is given in Table I with the low-temperature electronic specific heat coefficient γ. As a final result the k vectors of the Fermi surface are presented in Table II.

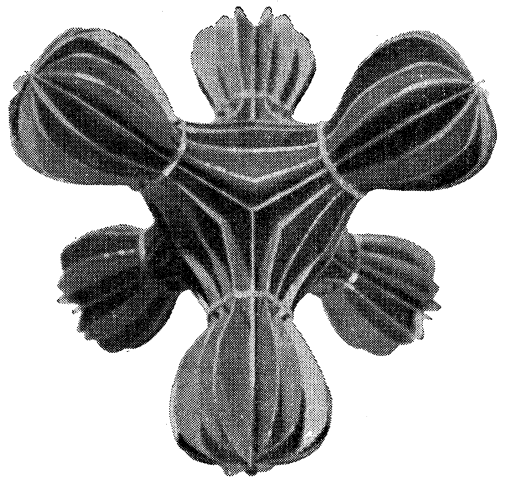

FIG. 5. Model of electron jack constructed from cross sections in Fig. 4.

DISCUSSION OF RESULTS

There are several relativistic effects on the Fermi surface of tungsten as determined from this theoretical calculation. The first is that the electron jack and hole octahedron are separated along the ΓH axis by the spin-orbit splitting of degenerate bands. The calculated splitting is in good agreement with the experimental results.[6] Spin-orbit splitting of degenerate bands also

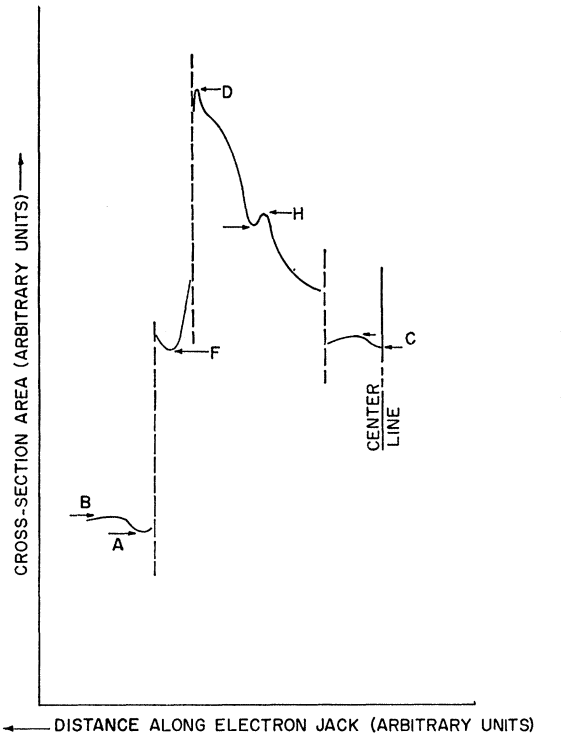

FIG. 6. Typical results for cross-sectional area of electron jack at different positions along a particular axis. Orientation of axis shown is 65° from the (001) direction in the (011) plane. Letters indicate extremal areas and correspond to de Haas–van Alphen frequencies in Fig. 7.

TABLE I. Some results of APW and RAWP calculations.

	RAPW	APW[a]	Experimental[b]
Tungsten			
E_F (Ry)	0.760	0.548	···
$G(E_F)$ (electrons/a.u. Ry)	0.0387	0.0673	···
γ (10^{-4} cal/mole deg^2)	1.72	2.98	3.1
Molybdenum			
E_F (Ry)	···	0.542	···
$G(E_F)$ (electrons/a.u.^{3} Ry)	···	0.0695	···
γ (10^{-4} cal/mole deg^2)	···	3.04	4.8

[a] Reference 8. [b] Reference 14.

causes the disappearance of the electron lenses inside the necks of the jack. Of course, it is possible that an improved potential (there was no attempt made toward self-consistency) or an expanded basis set would alter the bands and Fermi energy as shown in Fig. 1. A small change could produce very small electron lenses inside the necks of the jack. Even so, it is clear that they would be greatly reduced in size as compared with the nonrelativistic result.

Another theoretical result is the disappearance of the ellipsoidal holes at N. This was not the result of spin-orbit splitting, but instead was due to relativistic contributions to the effective potential. These effects are perhaps more familiar as the so-called mass-velocity and Darwin terms which result from successive applications of the Foldy-Wouthuysen transformation to the Dirac Hamiltonian. These first-order terms are not visibly displayed in our more general treatment, but effects of this kind are certainly present. Any energy levels which are very sensitive to the potential will therefore be shifted. The result in the present calculation is the disappearance of the holes at N. A similar result was predicted for chromium in NON-REL. In that instance the change in the potential was the result of less effective screening of the nuclear charge near the origin by the core electrons in chromium as compared to molybdenum and tungsten. It was, however, the same sensitive energy levels near the symmetry point N which were involved in both cases.

Actually there is experimental evidence which indicates that the holes at N have not disappeared completely but are greatly reduced in size. Sparlin[10] has measured de Haas–van Alphen frequencies with the appropriate angular dependence for the holes at N. These frequencies are in the range of 6.0 to 9.4 G. They are much smaller than the range 16.5 to 32.3 G as predicted in NON-REL.

TABLE II. k vectors of Fermi surface (atomic units^{-1}).

	Direction	APW	RAPW	Size-effect experiment[a]
Hole octahedron	(001)	0.45	0.41	0.41
	(011)	0.33	0.31	0.32
	(111)	0.28	0.26	0.27
Electron jack	(001)	0.61	0.57	0.59
	(011)	0.26	0.21	···
	(111)	0.23	0.19	0.22

[a] Walsh and Grimes, Ref. 7.

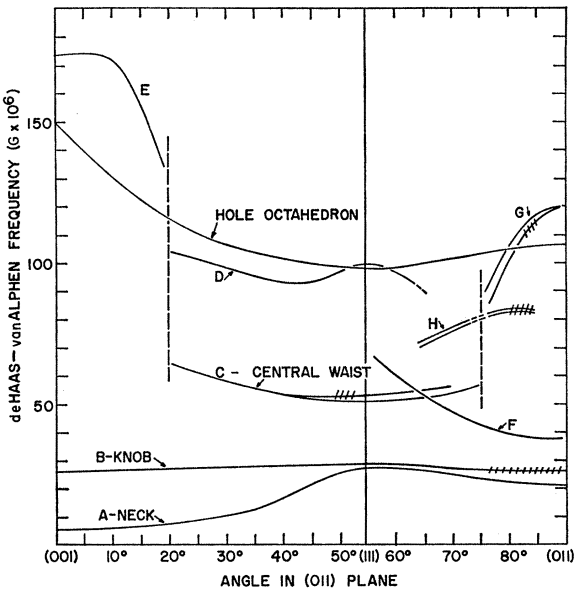

FIG. 7. de Haas–van Alphen frequencies predicted from relativistic Fermi surface of tungsten for magnetic field orientations in the (011) plane. Slashes indicate regions where beats are possible.

The primary relativistic effect on the electron jack is to reduce it in size and smooth out the neck region. The reduction in size of the knobs and necks is supported by the experimental results of Sparlin[10], Brandt and Rayne,[11] and Girvan.[12] The results of Sparlin are shown in Fig. 9 for comparison with the theoretical neck and knob orbits. The neck orbit predicted in NON-REL for the (100) direction was too large by nearly a factor of 2. These results are compared in Table III. We see that the relativistic shrinking of the knobs and neck is supported by the experimental

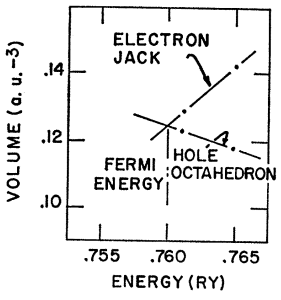

FIG. 8. Volume contained by electron jack and hole octahedron for two energies near the Fermi energy.

[10] D. M. Sparlin, thesis, Northwestern University, 1964 (unpublished).
[11] G. B. Brandt and J. A. Rayne, Phys. Rev. 132, 1945 (1963).
[12] R. F. Girvan, M. S. thesis, Iowa State University, 1964 (unpublished).

TABLE III. Tungsten de Haas–van Alphen frequencies (10^6 G).

	Direction and orbit	Theory APW	Theory RAPW	Experiment Sparlin[a]	Experiment Girvan[b]
Hole octahedron	(001)	168	149	150	152
	(011)	130	107	111	116
	(111)	108	98	104	104
Electron jack	(001) 4-Ball	227	172	...	...
	(001) Neck	11.3	5.6	6.1	...
	(001) Knob	33.6	24.0	22.7	23.4

[a] Reference 10. [b] Reference 12.

results. It is apparent from Table II that the hole octahedron is also reduced in size. However, the reduction is a relatively small percent of the nonrelativistic size. Although the reduction tends to bring the theoretical results into closer agreement with experimental results, it is evident from Figs. 7 and 9 that the relativistic hole octahedron yields de Haas–van Alphen frequencies about 5% smaller than the experimental results of Sparlin.[10] A similar comparison can be found with the size effect experiments of Walsh and Grimes.[7] As shown in Table II, the k vectors of the hole octahedron as calculated relativistically and nonrelativistically tend to bracket the experimental results, the relativistic results being smaller. However, the differences are small in either case. Comparison of the electron jack dimensions with size-effect measurements is also given in Table II.

de Haas–van Alphen data for the electron jack in tungsten are apparently not easy to obtain. We see from Fig. 7 that the larger frequencies expected from the jack are of the same order of magnitude as those from the hole octahedron. Because the extrema are very narrow for most of the jack orbits (Fig. 6), the signals from the hole octahedron would probably be much stronger and dominate the experimental results for the higher frequencies. The strongest signals from the jack should, however, come from the central waist orbits near the (111) direction because the extrema are flatter than for the other orbits. These frequencies are also lower than the ones from the hole octahedron and should not be as difficult to separate experimentally. Girvan[12] has measured these waist orbits, and the results are shown in Fig. 9. The angular dependence of our results (curve C in Fig. 7) is in close agreement with Girvan, but the theoretical waist is somewhat smaller than experimentally observed. The experimental results reported do not indicate the splitting into two frequencies near the (111) direction. Apparently the noncentral knob and body orbit (curve F) and the noncentral waist orbit (curve H) have not been experimentally observed.

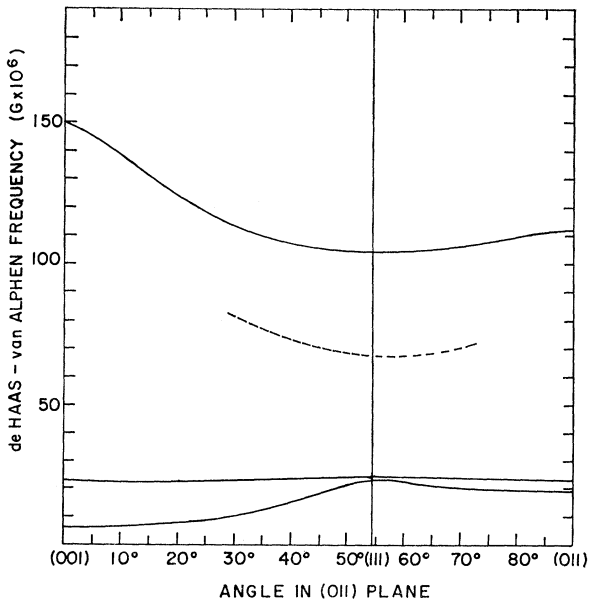

FIG. 9. Experimental de Haas–van Alphen frequencies: solid lines are results of Sparlin (Ref. 10) and dashed line is from Girvan (Ref. 12).

It is interesting to examine the shapes of the extremal areas for different angles along the curves E, D, and G of Fig. 7. For angles between 20° and 75° we consider curve D instead of C because portions of these orbits remain on the knobs. A typical extremal cross-section for curve E is shown in Fig. 10. It is sometimes referred to as the "4-ball" orbit. Also shown are typical extremal cross-sections corresponding to various angles along curve D. Starting at 30° a with "mouse," we arrive at the (111) direction with the "cloverleaf" orbit. A typical "2-ball" orbit for curve G is also shown in Fig. 10.

By now it is evident that relativistic effects have generally decreased the size of the Fermi surface. For most of the experimental results the relativistic surface is in better agreement than the one given in NON-REL, which was shown to be almost identical with the Fermi surface of molybdenum (see also Table I). Since these nonrelativistic theoretical surfaces are the same, and relativistic effects should be almost negligible in Mo, a comparison for these two metals of physical properties depending on the Fermi surface should indicate the extent of the relativistic effects. For instance the surface area of the Fermi surface, as determined by anomalous skin effect measurements, should be smaller for W than

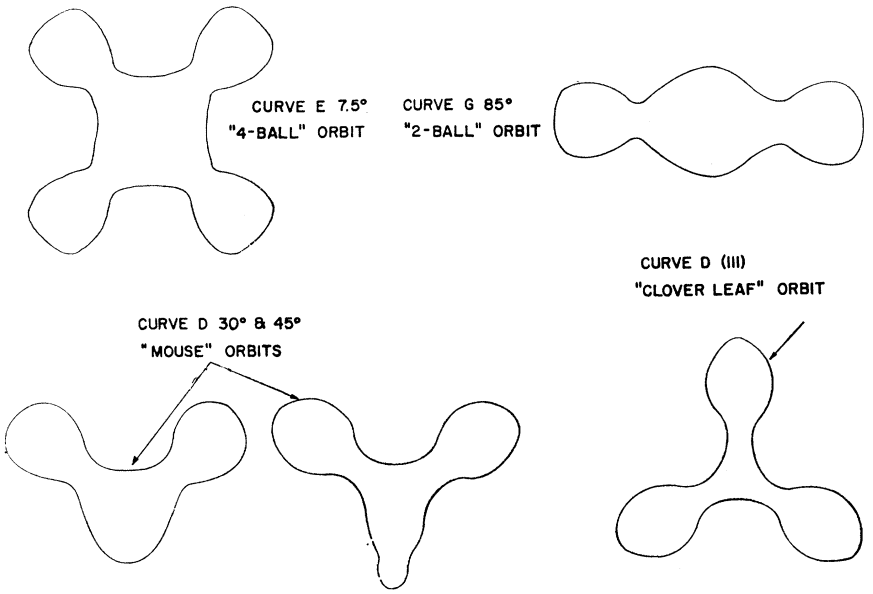

FIG. 10. Typical extremal cross-sections of electron jack corresponding to curves E, D, and G of Fig. 8.

Mo. Fawcett and Griffiths[13] have indeed measured 1.74 atomic units (a.u.) for the surface area of Mo and 1.66 a.u. for W. We have not accurately measured the surface area of the relativistic Fermi surface, but it is estimated to be about 7/10 of the nonrelativistic value 6.7 a.u. This difference is considerably more than is experimentally observed. However, not only the ratio of the Mo and W values differs from experiment, but also the individual magnitudes. As discussed in NON-REL, the anisotropy of the Fermi surface apparently makes it difficult to interpret the anomalous skin effect data for these metals.

Properties which depend on the density of states at the Fermi energy should, according to the results given for W in Table I, be very sensitive to relativistic effects. The apparent agreement in W between the APW results and experiment[14] is felt to be fortuitous. One obtains a more significant comparison if ratios of the quantities are examined. For instance, in Mo the ratio of γ (expt) to γ (APW) is 1.6. Since relativistic effects are not large in Mo, this would be about the same ratio if γ (RAPW) were used instead of γ (APW). However, for W the ratio γ (expt) to γ (APW) is only 1.0, whereas with γ (RAPW) we find 1.8. We thus find about the same enhancement in Mo and W (apparently due to the electron-phonon interaction) only if relativistic effects are considered for W.

From this we can conclude that the lower experimental value for W is due to relativistic effects. Shimizu, Takahashi, and Katsuki[15] also report the magnetic susceptibility (which is proportional to the density of state at the Fermi energy) for Mo and W. Their values have a ratio of about 1.5, which is further evidence that the density of states at the Fermi energy is decreased by relativistic effects.

We notice in Table I that the Fermi energy as measured from the bottom of the band is greater for the relativistic calculation. This results from the energy of the lower momentum states having been decreased by the relativistic contributions to the effective potential. In NON-REL we found the bandwidths of Mo and W to be nearly the same. It would be interesting to find experimental evidence to support this expected increase of the bandwidth of W compared to Mo.

Note added in proof. Further results on the electronic structure of W have been given by L. F. Mattheiss, Phys. Rev. **139**, A1893 (1965). His calculations were done using the nonrelativistic APW method. It is interesting that we agree on the nonrelativistic value of γ (Table I), but that the change attributed here to relativistic effects can equally well be accounted for by a 30% reduction of the exchange contribution to the potential. Such a reduction is certainly justified for states near the Fermi energy (see discussion by J. C. Slater, MIT Quarterly Progress Report No. 58, SSMTG (unpublished). Since both effects vary the *s-d* energy separation it is difficult to separate them. However,

[13] E. Fawcett and D. Griffiths, J. Phys. Chem. Solids **23**, 1631 (1962).

[14] *American Institute of Physics Handbook*, edited by D. E. Gray *et al.* (McGraw-Hill Book Company, Inc., New York, 1963), 2nd ed., pp. 4–61.

[15] M. Shimizu, T. Takahashi, and A. Katsuki, J. Phys. Soc. Japan **17**, 1740 (1962).

changes in the exchange potential should also affect the results for Mo and we have seen (Ref. 8) that this is not necessary to get agreement with experiment. This, coupled with the fact that Mo and W differ in several experiments, leads us to attribute these differences mainly to relativistic effects.

ACKNOWLEDGMENTS

Measurement of extremal areas of the electron jack was very carefully done by John Hinrichsen as part of his activities under the Summer Undergraduate Trainee Program at the Ames Laboratory.

PHYSICAL REVIEW VOLUME 143, NUMBER 2 MARCH 1966

Exciton Spectrum of ZnO

Y. S. PARK, C. W. LITTON, T. C. COLLINS, AND D. C. REYNOLDS
Aerospace Research Laboratories, Wright-Patterson Air Force Base, Ohio
(Received 4 October 1965)

The absorption and reflection spectra of ZnO crystals have been studied in the region of intrinsic absorption, and the data have been interpreted in terms of the wurtzite model given by Birman. Three intrinsic exciton transitions have been observed, one associated with each of the three valence bands. Several bound-exciton transitions have also been observed. The data have been analyzed, and a number of exciton parameters in ZnO are reported which are somewhat modified from those previously reported.

I. INTRODUCTION

THE fundamental exciton spectra of ZnO crystals was first investigated by Thomas.[1] He made a detailed study of the optical properties near the onset of intrinsic absorption and interpreted the data in terms of the wurtzite band structure derived by Birman.[2] The details of the band model are shown in Fig. 1. The conduction band is s-like, having Γ_7 symmetry. The valence band is p-like, splitting into three doubly degenerate bands due to spin-orbit and crystalline-field interactions. The top valence band has Γ_9 symmetry while the two lower valence bands have Γ_7 symmetry.

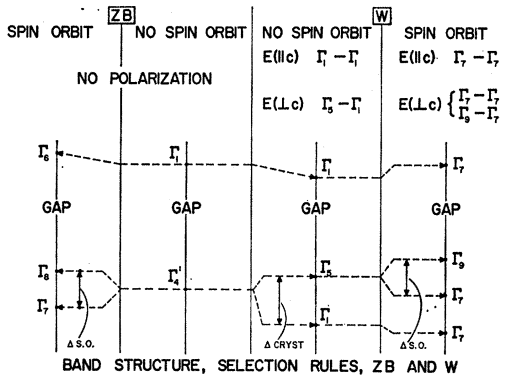

FIG. 1. Band structure and selection rules for zinc blende and wurtzite structures at the Γ symmetry point ($\mathbf{k}=0$). Crystal-field and spin-orbit splittings are indicated schematically. Transitions which are allowed for various polarizations of photon electric vector with respect to the crystalline "C" axis are indicated, i.e., $E\perp C$ or $E\|C$ (after Birman).

The selection rules allow a $\Gamma_7 \rightarrow \Gamma_9$ transition for light polarized in the orientation $E\perp C$; $\Gamma_7 \rightarrow \Gamma_7$ transitions are allowed for both modes of polarization ($E\perp C$ and $E\|C$).

From reflection spectra Thomas identified three exciton series, one associated with each of the three valence bands. The two top valence bands (A and B bands) are split by approximately 0.006 eV, and the third valence band (C band) is separated from the B band by 0.038 eV. In reflection, the excitons formed from the A and B bands were active for light polarized with the E vector perpendicular to the crystal C axis ($E\perp C$). Excitons formed from the C band were active for light polarized with the E vector parallel to the crystal C axis ($E\|C$). Thomas also observed from absorption experiments that transitions from the top valence band were at least partially polarized in the mode $E\|C$. Based on these polarization experiments, he concluded that the states from the first and third valence bands were mixed and that the symmetries of two top valence bands were reversed in ZnO. This behavior is quite different from what has been observed from similar experiments in other II–VI compounds. For example, in a detailed study of the optical properties of CdS crystals near the absorption edge, Thomas and Hopfield[3,4] developed a theory from Birman's model that successfully explained their intrinsic exciton data. The intrinsic exciton structure of CdSe was similarly explained by Wheeler and Dimmock,[5] and more recently

[1] D. G. Thomas, J. Phys. Chem. Solids **15**, 86 (1960).
[2] J. L. Birman, Phys. Rev. Letters **2**, 157 (1959).
[3] D. G. Thomas and J. J. Hopfield, Phys. Rev. **116**, 573 (1959).
[4] D. G. Thomas and J. J. Hopfield, Phys. Rev. **122**, 35 (1962).
[5] R. G. Wheeler and J. O. Dimmock, Phys. Rev. **125**, 1805 (1962).

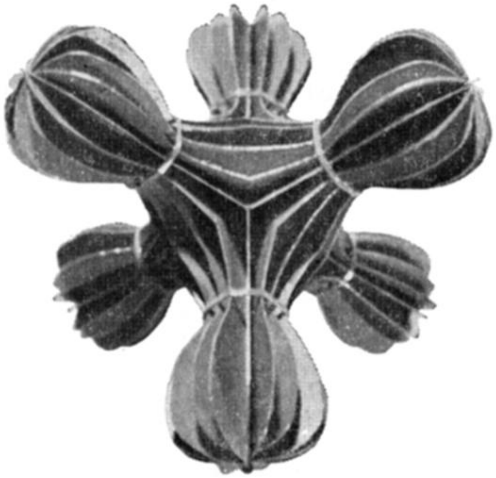

FIG. 5. Model of electron jack constructed from cross sections in Fig. 4.